

UC San Diego

UC San Diego Previously Published Works

Title

Collagen proton fraction from ultrashort echo time magnetization transfer (UTE-MT) MRI modelling correlates significantly with cortical bone porosity measured with micro-computed tomography (μ CT)

Permalink

<https://escholarship.org/uc/item/6cv6j7j7>

Journal

NMR in Biomedicine, 32(2)

ISSN

0952-3480

Authors

Jerban, Saeed
Ma, Yajun
Wan, Lidi
et al.

Publication Date

2019-02-01





DOI

10.1002/nbm.4045

Peer reviewed

RESEARCH ARTICLE

Collagen proton fraction from ultrashort echo time magnetization transfer (UTE-MT) MRI modelling correlates significantly with cortical bone porosity measured with micro-computed tomography (μ CT)

Saeed Jerban¹  | Yajun Ma¹  | Lidi Wan¹ | Adam C. Searleman¹ | Hyungseok Jang¹  | Robert L. Sah^{2,3} | Eric Y. Chang^{1,4} | Jiang Du¹ 

¹Department of Radiology, University of California, San Diego, CA, USA

²Department of Bioengineering, University of California, San Diego, CA, USA

³Department of Orthopaedic Surgery, University of California, San Diego, CA, USA

⁴Radiology Service, VA San Diego Healthcare System, San Diego, CA, USA

Correspondence

Jiang Du and Saeed Jerban, Department of Radiology, University of California, 9500 Gilman Dr, San Diego, CA 92093, USA.
Email: jiangdu@ucsd.edu; sjerban@ucsd.edu

Funding information

VA, Grant/Award Numbers: I01RX002604 and I01CX001388; NIH, Grant/Award Number: 1 R01 AR068987-01, 1R01 AR062581-01A1 and T32EB005970

Intracortical bone porosity is a key microstructural parameter that determines bone mechanical properties. While clinical MRI visualizes the cortical bone with a signal void, ultrashort echo time (UTE) MRI can acquire high signal from cortical bone, thus enabling quantitative assessments. Magnetization transfer (MT) imaging combined with UTE-MRI can indirectly assess protons in the bone collagenous matrix, which are inversely related to porosity. This study aimed to examine UTE-MT MRI techniques to evaluate intracortical bone porosity. Eighteen human cortical bone specimens from the tibial and fibular midshafts were scanned using UTE-MT sequences on a clinical 3 T MRI scanner and on a high-resolution micro-computed tomography (μ CT) scanner. A series of MT pulse saturation powers (500° , 1000° , 1500°) and frequency offsets (2, 5, 10, 20, 50 kHz) were used to measure the macromolecular fraction (MMF) and macromolecular T_2 (T_{2MM}) using a two-pool MT model. The measurements were made on 136 different regions of interest (ROIs). ROIs were selected at three cortical bone layers (from endosteum to periosteum) and four anatomical sites (anterior, mid-medial, mid-lateral, and posterior) to provide a wide range of porosity. MMF showed moderate to strong correlations with intracortical bone porosity ($R = -0.67$ to -0.73 , $p < 0.01$) and bone mineral density (BMD) ($R = +0.46$ to $+0.70$, $p < 0.01$). Comparing the average MMF between cortical bone layers revealed a significant increase from the endosteum towards the periosteum. Such a pattern was in agreement with porosity reduction and BMD increase towards the periosteum. These results suggest that the two-pool UTE-MT technique can potentially serve as a novel and accurate tool to assess intracortical bone porosity.

KEYWORDS

bone mineral density, cortical bone, magnetization transfer, micro-computed tomography, MRI, porosity, ultrashort echo time

Abbreviations used: 3D UTE, three-dimensional ultrashort echo time imaging; 3D, three dimensional; AFI-VTR, actual flip angle–variable T_R ; BMD, bone mineral density; CT, computed tomography; FA, flip angle; FOV, field of view; k , proton exchange rate constant; M_0 , fully relaxed magnetization; MM, macromolecules; MMF, macromolecular fraction; MT, magnetization transfer; R_1 , longitudinal rate constant; R_{1obs} , apparent longitudinal relaxation rate; ROI, region of interest; T_{2MM} , macromolecular T_2 ; T_E , echo time; T_R , repetition time; VTR, variable T_R ; μ CT, micro-computed tomography

1 | INTRODUCTION

Cortical bone plays a main role in load bearing and comprises around 80% of human bone mass.^{1,2} Intracortical bone porosity is an influential property for bone biomechanics and fracture risk prediction.^{3,4} Haversian canals (10–200 μm), lacunae (1–10 μm), and canaliculi (0.1–1 μm)^{5,6} are the three classes of pores existing in cortical bone, and average intracortical bone porosity may reach up to 20%.^{1,2,7} Bone porosity varies with age and various bone diseases such as osteoporosis.⁸

Cortical bone assessment has been widely performed using x-ray based techniques such as computed tomography (CT).^{1,7,9–15} MRI based assessment of cortical bone has received great attention to avoid potential harms associated with x-ray based techniques. However, clinical MRI is not able to detect a considerable signal from cortical bone because of its very short apparent transverse relaxation time (T_2^*).^{1,2,16,17}

Ultrashort echo time (UTE) MRI can image cortical bone^{1,2,7,9–14,18–24} and other tissues with low transverse relaxation times.^{1,25,26} With UTE-MRI, signal can be acquired after RF excitation, as quickly as allowed by the RF hardware (tens of microseconds), before major decay in transverse magnetization. In addition to morphological imaging, UTE-MRI allows for quantitative assessment of cortical bone.

At least three hydrogen proton pools with different T_2^* values are present in bone: (1) collagen backbone protons, (2) bound water, and (3) pore water and lipid.^{2,7,27,28} The associated T_2^* values for the aforementioned proton pools, on a 3 T MR scanner, are less than 50 μs , 300–400 μs , and more than 1 ms, respectively.^{1,2,7} The T_2^* of collagen backbone protons are extremely short and are challenging to image directly with current MRI scanners.²⁹

Magnetization transfer (MT) imaging combined with UTE-MRI has been recently introduced as a technique to indirectly measure protons in collagenous matrix relative to water protons.^{19,23,30–32} With MT techniques, a high-power saturation RF pulse (such as a Fermi type pulse) is used with a defined frequency offset from the water protons' resonance frequency to saturate mainly protons in collagenous matrix. The saturated MTs from the collagenous matrix to water protons can be detected by UTE-MRI. The magnitude of the saturation transferred to water protons correlates with the number of collagen protons relative to water protons in the tissue. The complexity of UTE-MT measurements may range from a simple MT ratio^{30,32} to macromolecular fraction (MMF) and T_2 ($T_{2\text{MM}}$) obtained from a two-pool UTE-MT model.^{19,23,31,33}

UTE-MT estimation of collagen protons relative to water protons is assumed to be correlated with cortical bone porosity and the mechanical properties of the bone. MT ratio derived from 2D UTE-MT imaging has been shown to be significantly correlated with μCT based cortical bone porosity.³⁰ Higher MT ratios indicate more saturation transferred to the water pool, implying less water and porosity in bone. However, describing collagen content would be challenging based on MT ratios, because the ratios significantly vary for different RF pulse powers and frequency offsets.

In a two-pool UTE-MT model, the fraction of collagen protons (i.e. MMF) can be obtained using a set of RF pulse powers and frequency offsets.^{19,31,33} MMF is assumed to represent the bone matrix volume, whereas the water pool fraction indicates the total water existing in the bone, which may correlate with bone porosity. Thus, the two-pool UTE-MT technique has the potential to diagnose certain bone diseases associated with porosity variation such as osteoporosis. More importantly, for diseases affecting bone collagenous matrix and bone minerals differently, such as osteomalacia,³⁴ the two-pool UTE-MT technique can provide information complementary to bone mineral density (BMD) measurements. Recently, the two-pool UTE-MT technique has been utilized to detect ex vivo fibular bone stress injury induced cyclic loading where the bone collagenous matrix is affected despite an unchanged BMD.²³ MMF demonstrated a significant reduction after the induced partial bone stress injury.²³ Nevertheless, the relationship between UTE-MT measures and intracortical bone porosity needs to be determined prior to investigating the clinical performance of UTE-MT methods.

The purpose of this study was to investigate the relationship between the two-pool UTE-MT measures and intracortical bone porosity as measured using high-resolution micro-computed tomography (μCT). This study helps to highlight the potential applications of UTE-MT methods for assessing intracortical porosity in the human skeleton.

2 | MATERIALS AND METHODS

2.1 | Sample preparation

Eighteen cortical bone specimens were harvested from fresh-frozen human tibial ($n = 9$, 63 ± 19 years old, five women and four men) and fibular ($n = 9$, 52 ± 18 years old, three women and six men) midshafts, provided by a non-profit whole-body donation company (United Tissue Network, Phoenix, AZ, USA). Bone specimens were cut to 25 mm in length using a Delta ShopMaster bandsaw (Delta Machinery, Jackson TN, USA).

2.2 | UTE-MRI

All bone specimens were immersed in phosphate-buffered saline (PBS) for 2 h at room temperature before the MRI scans. Specimens were placed in a plastic container filled with perfluoropolyether (Fomblin, Ausimont, Thorofare, NJ, USA) to minimize dehydration and susceptibility artifacts. The UTE-MRI scans were performed on a 3 T clinical scanner (MR750, GE Healthcare Technologies, Milwaukee, WI, USA) using an eight-channel knee coil for both RF transmission and signal reception. The UTE-MRI scans involved the following two quantitative protocols: (A) an actual flip

angle–variable T_R (AFI-VTR) based three-dimensional (3D) UTE-Cones sequence (AFI $T_E = 0.032$ ms, $T_R = 20$ and 100, flip angle (FA) = 45°; VTR $T_E = 0.032$ ms, $T_R = 20, 30, 50,$ and 100 ms, FA = 45°, rectangular RF pulse with a duration of 150 μ s) for T_1 measurement, which is a prerequisite for accurate MT modeling,³⁵ and (B) a three-dimensional ultrashort echo time imaging (3D UTE)-Cones-MT sequence (Fermi saturation pulse power = 500°, 1000°, and 1500°, frequency offset = 2, 5, 10, 20, and 50 kHz, FA = 7°, nine spokes were acquired after each MT preparation; rectangular RF excitation pulse with a duration of 26 μ s) for two-pool MT modeling. Details of the 3D UTE-Cones sequence are given in previous studies.^{36–38} Field of view (FOV), matrix dimension, nominal in-plane pixel size, and slice thickness were 140 × 140 mm², 256 × 256, 0.54 × 0.54 mm², and 2 mm for tibial specimens, respectively. Fibular specimens are much smaller than tibial specimens; therefore, to improve the resolution for fibular specimens, FOV, matrix dimension, pixel size, and slice thickness were 100 × 100 mm², 256 × 256, 0.39 × 0.39 mm², and 4 mm, respectively. FOVs were selected in the range used for in vivo studies. This helps future translational study of cortical bone in human subjects. Moreover, these larger FOVs enabled scanning a few samples together in one container.

2.3 | μ CT

All 18 bone specimens were scanned using a Skyscan 1076 (Kontich, Belgium) μ CT scanner at 8.78 μ m isotropic voxel size. For measuring BMD in addition to bone porosity, specimens were scanned in the presence of two hydroxyapatite phantoms (0.25 and 0.5 g/cm³). Other scanning parameters were as follows: a 0.05 mm aluminum plus 0.038 mm copper filter, 100 kV, 100 mA, 0.4° rotation step, and 5 times frame-averaging. μ CT scan time was 6 h.

2.4 | Data analysis and statistics

UTE-MT results in one slice in the middle of the specimens were compared with the μ CT based measures in the corresponding number of slices (222 and 444 for tibial and fibular specimens, respectively). The comparison between MRI and μ CT results was performed within 12 and 4 regions of interest (ROIs) for tibial and fibular specimens, respectively. Finally, Pearson's correlations were calculated between UTE-MT results and μ CT based measures (cortical bone porosity and BMD). Moreover, UTE-MT and microstructural results were compared between different layers of the cortical bone from the endosteum towards the periosteum. Specifically, average values associated with each cortical bone layer were compared with those of other layers using the two-tailed paired Student *t*-test. *p* values below 0.05 ($\alpha = 0.05$) were considered significant. Multiple comparison correction based on Holm approach was applied after ordering the calculated *p* values in ascending order. All statistical analyses were performed using Microsoft Excel (Version 2013, Microsoft Corporation, WA, USA).

ROIs were selected by a medical imaging expert in different cortical bone layers and anatomical sites on the UTE images. This approach for ROI selection provided an adequate range of porosity in bone to examine the presented techniques. Figure 1A shows schematically the 12 selected ROIs in a representative tibia sample at three cortical bone layers (from endosteum to periosteum) and four anatomical sites (anterior, mid-medial, mid-lateral, and posterior). Likewise, Figure 1B shows schematically the four selected ROIs in a representative fibula sample in two cortical bone layers and two anatomical sites (medial and lateral).

2.4.1 | UTE-MT modeling

The data acquired with the set of MT saturation pulse powers (500°, 1000°, and 1500°) and frequency offsets (2, 5, 10, 20, and 50 kHz) were fitted by a modified rectangular pulse approximation (mRP) approach that had been previously described.^{19,31,33} In the two-pool model, cortical

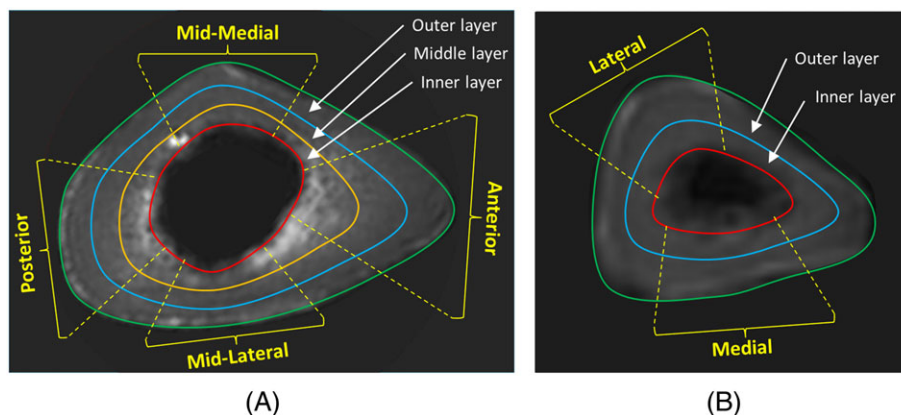


FIGURE 1 Schematic diagrams of selected ROIs in UTE-MRI images. A, twelve selected ROIs depicted on the UTE-MRI image of a representative tibial bone specimen (male, 73 years old). B, four selected ROIs depicted on the UTE-MRI image of a representative fibular bone specimen (male, 54 years old)

bone is assumed to have two different proton pools. The first pool is the macromolecular proton pool, which has a very broad spectrum or extremely short T_2 (~ 10 μs). The second pool is the water proton pool, which includes both bound and pore water protons. Protons of the two pools in this model are continuously exchanging their magnetizations. If the macromolecular proton magnetization is partially saturated, the acquired water signal intensity decreases due to the MT. A two-pool MT model can be built based on the Bloch equation such that the signal in UTE-MT is given as a function of MMF and following MRI properties of the two pools. Considered MRI properties in this model are (1) the fully relaxed magnetization of the macromolecular pool (M_{0m}) and water pool (M_{0w}), (2) the longitudinal rate constants of the macromolecular pool (R_{1m}) and water pool (R_{1w}), (3) the proton exchange rate constant between the two pools (k), and (4) the loss rate of longitudinal magnetization of the macromolecular pool.^{19,31,33} A Gaussian line shape was used to model the macromolecular proton spectrum. The loss of the longitudinal magnetization of the macromolecular pool was also fitted by a Gaussian line shape function.³¹ As a prerequisite for UTE-MT modeling, T_1 was measured using a recently developed 3D UTE AFI-VTR method on acquired UTE images with variable T_R for B_1 error correction.³⁵

The UTE-MT analysis was performed offline on the acquired DICOM images using an in-house code written in MATLAB (Version 2016, MathWorks, Natick, MA, USA). A Levenberg–Marquardt algorithm was employed for the non-linear least-squares fitting in both UTE-MT modeling and T_1 fitting within the earlier selected ROIs (Figure 1).

2.4.2 | Bone porosity and mineral density measurements

A single gray level threshold was used for μCT image segmentation to distinguish between bone and pores. The gray level threshold was selected for each set of μCT data using the peaks of gray level histograms and visual inspection of the raw images. Thresholding resulted in a stack of binary images. A porosity pixel map was generated for each bone specimen by superimposing the corresponding number of binary images (222 and 444 slices for tibial and fibular specimens, respectively). BMD was calculated for each voxel by comparing its gray level with the average gray level of the scanned hydroxyapatite phantom with known density (0.25 and 0.5 g/cm^3). BMD pixel map was then generated by averaging the BMD values in the corresponding number of images. Afterwards, the average bone porosity and BMD were calculated within each ROI. Affine image registration was used to propagate the ROIs used for MRI analysis to the μCT data.

3 | RESULTS

Figure 2A and 2B show the axial UTE-MRI and μCT images of a representative tibial bone specimen (male, 73 years old), respectively. Likewise, Figure 2C and 2D shows the axial UTE-MRI and μCT images of a representative fibula bone specimen (male, 54 years old), respectively. A 20% water phantom is placed in the center of the tibial specimen shown in Figure 2A for calibration purposes and to evaluate bone water content

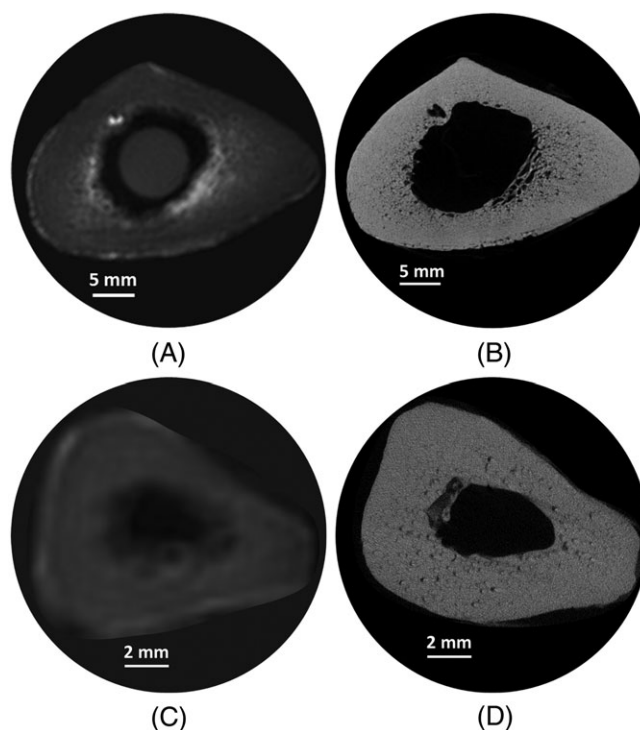


FIGURE 2 A, B, UTE-MRI (A) and μCT (B) images of a representative tibial bone specimen in the axial plane (male, 73 years old). C, D, UTE-MRI (C) and μCT (D) images of a representative fibular bone specimen in the axial plane (male, 54 years old). A 20% water phantom is shown in the center of the tibial specimen (A) for calibration purposes and to evaluate bone water content to be followed in future steps

to be followed in future steps. The samples in UTE-MRI images (Figure 2A and 2C) were cropped for presentation purposes to avoid showing other specimens in the FOV.

Figure 3A shows a magnified μ CT image of a representative tibial bone specimen focused on the anterior tibia. Porosity and BMD are measured for two selected ROIs in middle and outer layer of the cortex. Two-pool MT modeling analysis of the selected ROIs are shown in Figure 3B and 3C, respectively, using the three MT saturation pulse powers (500° , 1000° , and 1500°) and five off-resonance frequencies (2, 5, 10, 20, and 50 kHz).

Pearson's correlation coefficients between UTE-MRI markers (T_1 , MMF, and T_{2MM}) and μ CT measures (bone porosity and BMD) are presented in Table 1. MMF showed moderate to strong correlations with bone porosity ($R = -0.67$ to -0.73 , $p < 0.01$) and BMD ($R = +0.46$ to $+0.70$, $p < 0.01$) as measured with μ CT for all bone specimens regardless of the tibia or fibula harvest location.³⁹ The numbers of data points for correlation calculation were the numbers of analyzed ROIs and were equal to 108 and 36 for tibial and fibular specimens, respectively. T_{2MM} did not demonstrate significant correlations with bone porosity or BMD ($p > 0.05$). T_1 showed a moderate and consistent correlation with μ CT based bone porosity for both tibial ($R = +0.56$) and fibular ($R = +0.60$) bone specimens. However, only a poor correlation was found between T_1 and BMD ($R = -0.16$ to -0.47 , $p < 0.01$, Table 1).

Figure 4A and 4B demonstrates the scatter plot and the linear regressions of MMF on bone porosity and BMD as measured with μ CT, respectively, for all tibial bone specimens. Likewise, Figure 4C and 4D shows the regressions of MMF for all fibular specimens. The linear regressions of MMF on bone porosity and BMD, when considering all bone specimens, are shown in Figure 4E and 4F, respectively.

Figure 5A-C shows MMF (from UTE-MT modeling), bone porosity, and BMD (as measured with μ CT) pixel maps for a representative tibial specimen (male, 73 years old), respectively. Similarly, Figure 5D-F presents pixel maps for a representative fibular bone specimen (male, 54 years old). Regions of higher MMF in tibial and fibular samples (Figure 5A and 5D) corresponded to the regions of lower porosity in the porosity maps (Figure 5B and 5E). To avoid the pixelation effect in the presented maps, MMF, porosity, and BMD maps were smoothed using a Gaussian filter in 3×3 , 5×5 , and 5×5 sub-windows, respectively.

Table 2 presents the variations of microstructural properties and UTE-MT biomarkers between different selected layers in cortical bone. μ CT based porosity showed a significant reduction from the inner layer towards the outer layer of the cortex for both tibial and fibular bone specimens ($p < 0.01$). In contrast, BMD, MMF, and T_1 showed significant increases from the inner layer towards the outer layer ($p < 0.01$). T_{2MM} demonstrated no significant variation between selected cortical bone layers (Figure 1). Applying multiple comparison correction based on the Holm approach resulted in a 0.025 threshold for p values to be considered significant.

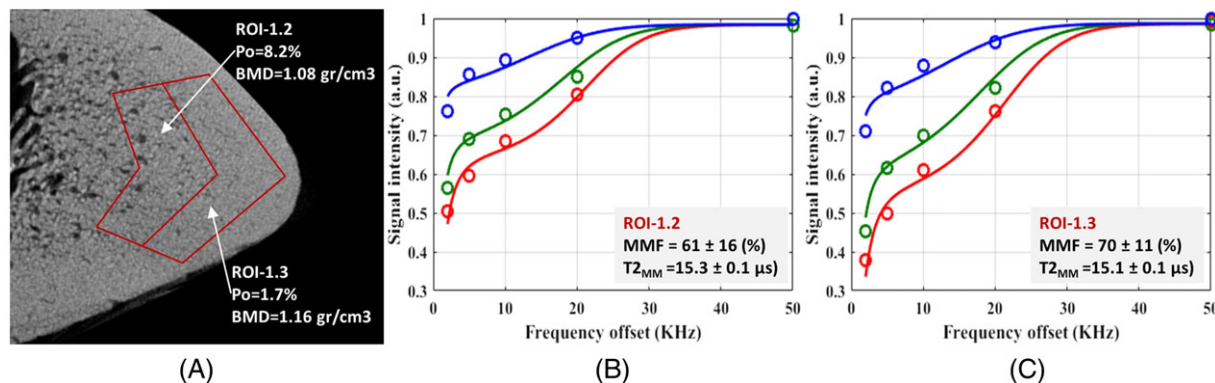


FIGURE 3 A, μ CT image of a representative tibial specimen (male, 73 years old) focused on anterior tibia with two selected ROIs in middle and outer layers. Measured porosity (Po) in the middle layer (ROI-1.2) is higher than that in the outer layer (ROI-1.3). B, C, the two-pool MT modeling analyses in ROI-1.2 (B) and ROI-1.3 (C) using three pulse saturation powers (500° in blue, 1000° in green, and 1500° in red) and five frequency offsets (2, 5, 10, 20, 50 kHz)

TABLE 1 Pearson's correlations between UTE-MT modeling results and μ CT based bone porosity and mineral density measures

		Two-pool MT modeling		
		T_1 (ms)	MMF (%)	T_{2MM} (μ s)
Porosity (%)	Tibia	0.56	-0.73	0.10
	Fibula	0.60	-0.67	0.49
	All	0.53	-0.70	0.26
BMD (g/cm^3)	Tibia	-0.36	0.70	-0.04
	Fibula	-0.47	0.61	-0.54
	All	-0.16	0.46	-0.29

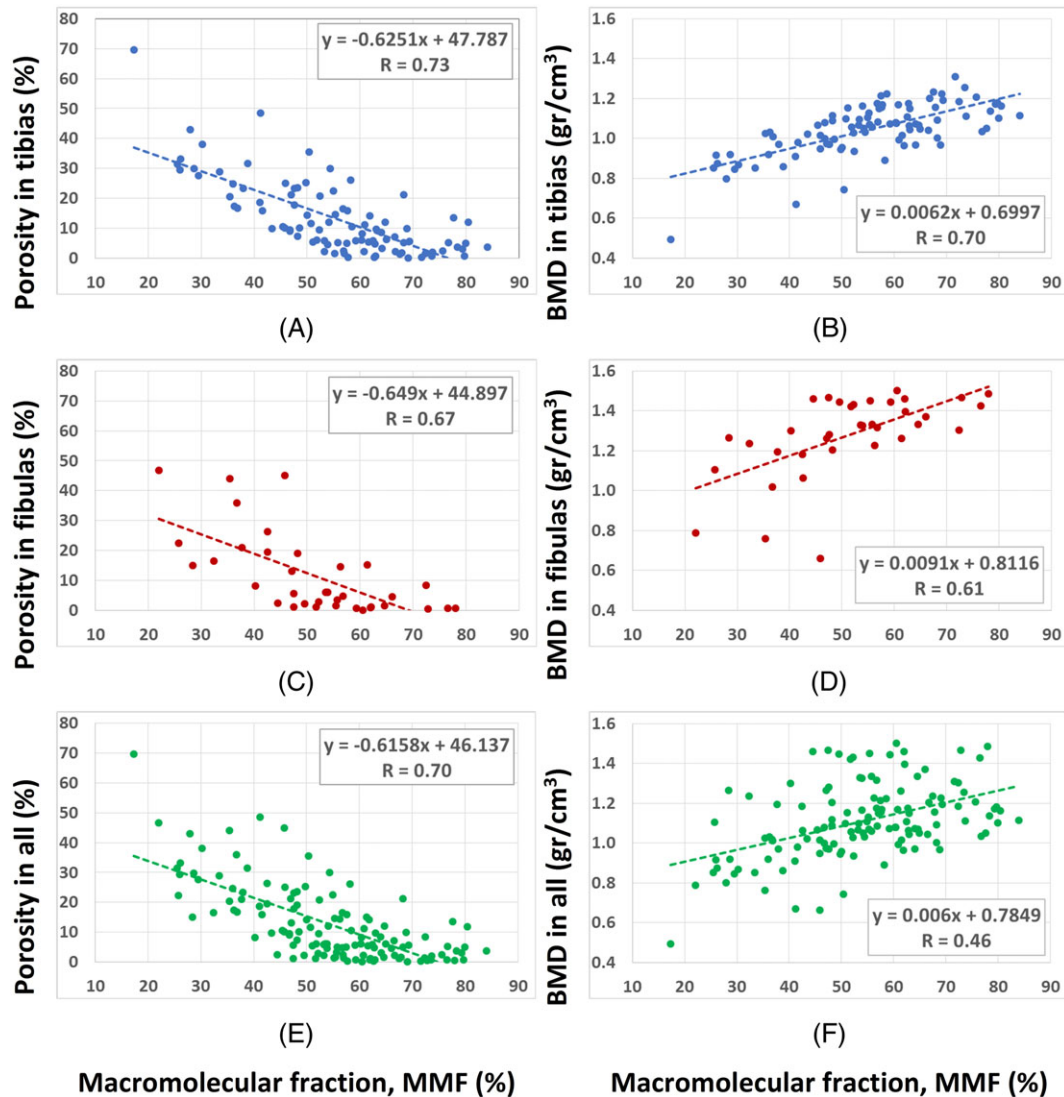


FIGURE 4 Significant ($p < 0.01$) correlation between MMF measure and microstructural properties of cortical bone specimens. A, C, E, scatter plot and linear regressions of MMF on bone porosity considering only tibial (a), only fibular (C), and all bone specimens (E). B, D, F, scatter plot and linear regressions of MMF measure and BMD considering only tibial (B), only fibular (D), and all bone specimens (F)

4 | DISCUSSION

This study has focused on recently developed UTE-MT based measures of collagenous matrix for ex vivo assessment of intracortical bone porosity. UTE-MT modeling techniques can provide an estimation of the collagen content in cortical bone.^{19,31,33,40} It is assumed that such estimation of the collagenous matrix content correlates with bone viscoelastic properties such as mechanical toughness. It is hypothesized that the bone porosity and bone volume density (or mineral density) are correlated with the collagen content in bone.

Previous UTE based assessments of the bone microstructure have been reported by focusing only on water hydrogen pools. The pore water pool has been estimated for its potential correlation with porosity through the following three approaches. First, T_2^* decay analysis using a bi-component exponential model to distinguish and evaluate the pore and bound water fractions in bone.^{2,41} Using this technique, pore water fractions presented good correlations with μ CT based porosity in bone.⁴¹ Second, the signal ratio between the UTE image and an image with longer T_E (i.e. 2 ms), the so-called porosity index, was used by Rajapakse et al. to estimate pore water fraction.¹⁰ Porosity index also demonstrated good correlation with μ CT based porosity.¹⁰ Third, UTE imaging after bound water saturation was used to estimate the pore water content through comparing the signal in bone with the signal of an external water reference (i.e. 10% H₂O plus 90% D₂O).²⁰ Estimated pore water content showed good correlation with μ CT based porosity.¹⁴

This study was the first investigation to draw correlations between the bone microstructural parameters and MMF, obtained from a two-pool UTE-MT model. UTE-MT modeling focuses on evaluation of the collagenous matrix of the bone for its potential applications in predicting viscoelastic properties. Chang et al.³⁰ showed earlier that the MT ratio from 2D radially acquired MT images correlates significantly with bone porosity. Although MT ratio and UTE-MT modeling share similar principles, describing collagen content would be challenging based on MT ratios, since the ratios vary significantly for different RF pulse powers and frequency offsets.

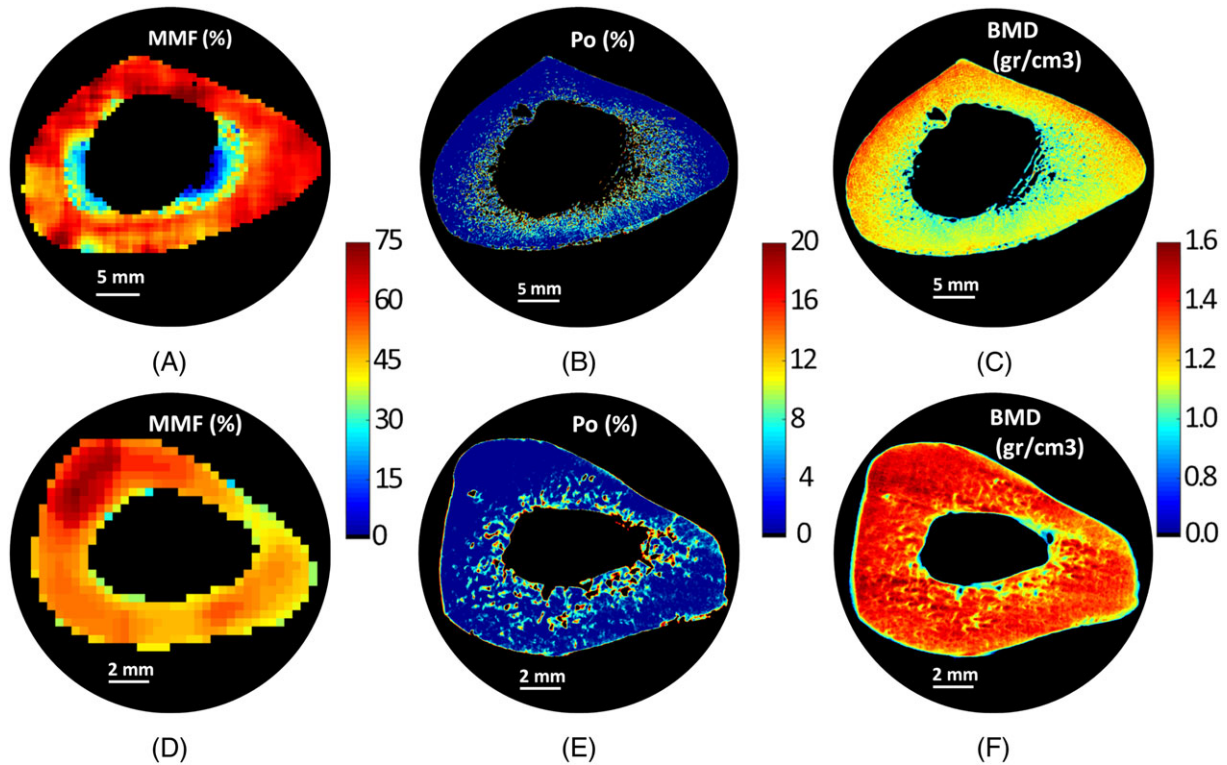


FIGURE 5 A-C, MMF (a), bone porosity (B), and BMD (C) maps of a representative tibial bone specimen (male, 73 years old). D-F, MMF (D), bone porosity (E), and BMD (F) maps of a representative fibular bone specimen (male, 54 years old)

TABLE 2 Variation (mean \pm SD) of bone microstructure and UTE-MT measures between selected cortex layers in tibia and fibula

		μ CT-based microstructure			Two-pool MT modeling	
		Porosity (%)	BMD (g/cm ³)	T_1 (ms)	MMF (%)	T_2 (μ s)
Tibias	Inner layer	25 \pm 14	0.94 \pm 0.13	238 \pm 24	46 \pm 16	15.0 \pm 0.4
	Middle layer	11 \pm 8	1.07 \pm 0.08	227 \pm 15	57 \pm 11	15.0 \pm 0.3
	Outer layer	6 \pm 5	1.12 \pm 0.08	209 \pm 14	65 \pm 9	14.9 \pm 0.3
	P-value (in vs mid)	<0.01	<0.01	<0.01	<0.01	0.22
	P-value (mid vs out)	0.01	<0.01	0.02	<0.01	0.35
Fibulas	Inner layer	19 \pm 18	1.21 \pm 0.25	250 \pm 22	46 \pm 12	15 \pm 0.7
	Outer layer	6 \pm 5	1.35 \pm 0.1	227 \pm 23	56 \pm 13	15 \pm 0.5
	P-value (in vs out)	<0.01	0.01	<0.01	<0.01	0.39

To validate the correlations between the UTE-MT measures and bone microstructural properties, μ CT was used for bone porosity and BMD measurements. From the two-pool UTE-MT modeling, MMF presented a strong negative correlation with bone porosity and moderate positive correlation with BMD for ROIs in tibial specimens (Table 1, Figure 5). Similarly, the MMF correlation coefficients in fibular specimens with bone porosity and BMD were moderate to high. Such consistently moderate to high correlations indicated that the MMF enables accurate detection of bone microstructural variations regardless of the type of the long bone. T_{2MM} did not demonstrate consistently good correlations with either bone porosity or BMD (Table 1). T_1 presented consistently moderate correlations with bone porosity; however, its correlations with BMD were poor (Table 1).

The variations of UTE-MT biomarkers and microstructural properties between different selected cortical layers were also investigated through this study (Figure 1). MMF showed a significant increase from inner towards the outer layers of the cortex for both tibial and fibular bone specimens ($p < 0.01$). MMF variations between bone layers agreed with the porosity variation pattern measured by μ CT. Porosity significantly decreased towards the outer layer of the cortex for both tibial and fibular bone specimens ($p < 0.01$). BMD and T_1 showed significant increases from the inner layer towards the outer layer ($p < 0.01$). Such results were in agreement with the multiple previous studies that have shown lower intracortical porosity and pore size on the periosteal side compared with the endosteal side, using a variety of methods including high-resolution microscopy, histology, and high-resolution quantitative CT.⁴²⁻⁴⁵

The results of this study suggested that MMF from UTE-MT modeling is a useful and promising surrogate for assessing human intracortical porosity and BMD in particular for specimens from donors with no known bone disease. This MRI based technique is non-invasive, x-ray free, and importantly translatable to in vivo studies. Focusing on the collagen matrix of the bone instead of the mineral density would be valuable

for evaluating the bone viscoelastic properties. Moreover, certain bone diseases may demonstrate variations in the collagenous matrix prior to changes in bone minerals.

This study was performed on ex vivo bone specimens where the bone marrow and surrounding muscles were removed. A well-designed in vivo study should be performed to examine similar correlations between UTE-MT measurements and bone porosity and BMD. Penetration of bone marrow fat into large pores of the cortex would be challenging for two-pool UTE-MT modeling. Considering three-pool UTE-MT modeling will be a promising path in future studies. Additionally, different fat suppression techniques followed by two-pool MT modeling would be an alternative for future in vivo studies. Optimizing fat suppression to minimize contamination of the water proton signal would be a crucial prerequisite on this path. Furthermore, the correlation of UTE-MT measures with biomechanics of cortical bone is very interesting and remains to be investigated.

5 | CONCLUSION

Two-pool UTE-MT modeling was investigated for its capability to assess intracortical bone porosity in an ex vivo study performed on human tibial and fibular midshafts. MMF obtained from MT modeling, as a quantification for collagenous matrix content, showed strong correlations with bone porosity and BMD. The correlations were consistently high for both tibial and fibular bone specimens, insensitive to the type of long bone. MMF showed a significant increase from endosteum towards periosteum in the cortex for both tibial and fibular specimens. The MMF variation between the cortical bone layers was in agreement with porosity reduction and BMD increase towards the periosteum. This study has highlighted UTE-MT MRI techniques as useful methods to assess intracortical bone porosity, which may be used in future clinical studies.

ACKNOWLEDGEMENTS

The authors acknowledge grant support from the NIH (1R01 AR062581-01A1, 1 R01 AR068987-01, and T32EB005970) and the VA (I01CX001388 and I01RX002604).

CONFLICTS OF INTEREST

The authors have no conflicts of interest to declare.

ORCID

Saeed Jerban  <https://orcid.org/0000-0001-6450-2892>

Yajun Ma  <https://orcid.org/0000-0003-0830-9232>

Hyungseok Jang  <https://orcid.org/0000-0002-3597-9525>

Jiang Du  <https://orcid.org/0000-0002-9203-2450>

REFERENCES

1. Chang EY, Du J, Chung CB. UTE imaging in the musculoskeletal system. *J Magn Reson Imaging*. 2015;41(4):870-883. <https://doi.org/10.1002/jmri.24713>
2. Du J, Bydder GM. Qualitative and quantitative ultrashort-TE MRI of cortical bone. *NMR Biomed*. 2013;26(5):489-506. <https://doi.org/10.1002/nbm.2906>
3. Granke M, Makowski AJ, Uppuganti S, Does MD, Nyman JS. Identifying novel clinical surrogates to assess human bone fracture toughness. *J Bone Miner Res*. 2015;30(7):1290-1300. <https://doi.org/10.1002/jbmr.2452>
4. Treece GM, Gee AH, Tonkin C, et al. Predicting hip fracture type with cortical bone mapping (CBM) in the osteoporotic fractures in men (MrOS) study. *J Bone Miner Res*. 2015;30(11):2067-2077. <https://doi.org/10.1002/jbmr.2552>
5. Cowin SC. Bone poroelasticity. *J Biomech*. 1999;32(3):217-238. [https://doi.org/10.1016/S0021-9290\(98\)00161-4](https://doi.org/10.1016/S0021-9290(98)00161-4)
6. Wang X, Ni Q. Determination of cortical bone porosity and pore size distribution using a low field pulsed NMR approach. *J Orthop Res*. 2003;21(2):312-319. [https://doi.org/10.1016/S0736-0266\(02\)00157-2](https://doi.org/10.1016/S0736-0266(02)00157-2)
7. Seifert AC, Wehrli FW. Solid-state quantitative ^1H and ^{31}P MRI of cortical bone in humans. *Curr Osteoporos Rep*. 2016;1-10. <https://doi.org/10.1007/s11914-016-0307-2>
8. Cooper DML, Kawallak CE, Harrison K, Johnston BD, Johnston JD. Cortical bone porosity: what is it, why is it important, and how can we detect it? *Curr Osteoporos Rep*. 2016;14(5):187-198. <https://doi.org/10.1007/s11914-016-0319-y>
9. Chang EY, Bae WC, Statum S, Du J, Chung CB. Effects of repetitive freeze-thawing cycles on T2 and T2* of the Achilles tendon. *Eur J Radiol*. 2014;83(2):349-353. <https://doi.org/10.1016/j.ejrad.2013.10.014>
10. Rajapakse CS, Bashoor-Zadeh M, Li C, Sun W, Wright AC, Wehrli FW. Volumetric cortical bone porosity assessment with MR imaging: validation and clinical feasibility. *Radiology*. 2015;276(2):526-535. <https://doi.org/10.1148/radiol.15141850>
11. Granke M, Does MD, Nyman JS. The role of water compartments in the material properties of cortical bone. *Calcif Tissue Int*. 2015;97(3):292-307. <https://doi.org/10.1007/s00223-015-9977-5>
12. Nyman JS, Ni Q, Nicoletta DP, Wang X. Measurements of mobile and bound water by nuclear magnetic resonance correlate with mechanical properties of bone. *Bone*. 2008;42(1):193-199. <https://doi.org/10.1016/j.bone.2007.09.049>

13. Du J, Hermida JC, Diaz E, et al. Assessment of cortical bone with clinical and ultrashort echo time sequences. *Magn Reson Med*. 2013;70(3):697-704. <https://doi.org/10.1002/mrm.24497>
14. Manhard MK, Uppuganti S, Granke M, Gochberg DF, Nyman JS, Does MD. MRI-derived bound and pore water concentrations as predictors of fracture resistance. *Bone*. 2016;87:1-10. <https://doi.org/10.1016/j.bone.2016.03.007>
15. Graeff C, Marin F, Petto H, et al. High resolution quantitative computed tomography-based assessment of trabecular microstructure and strength estimates by finite-element analysis of the spine, but not DXA, reflects vertebral fracture status in men with glucocorticoid-induced osteoporosis. *Bone*. 2013;52(2):568-577. <https://doi.org/10.1016/j.bone.2012.10.036>
16. Manhard MK, Nyman JS, Does MD. Advances in imaging approaches to fracture risk evaluation. *Transl Res*. 2017;181:1-14. <https://doi.org/10.1016/j.trsl.2016.09.006>
17. Hendeel WR, Morgan CJ. Magnetic resonance imaging. Part I—physical principles. *West J Med*. 1984;141(4):491-500.
18. Du J, Carl M, Bydder M, Takahashi A, Chung CB, Bydder GM. Qualitative and quantitative ultrashort echo time (UTE) imaging of cortical bone. *J Magn Reson*. 2010;207(2):304-311. <https://doi.org/10.1016/j.jmr.2010.09.013>
19. Ma Y-J, Shao H, Du J, Chang EY. Ultrashort echo time magnetization transfer (UTE-MT) imaging and modeling: magic angle independent biomarkers of tissue properties. *NMR Biomed*. 2016;29(11):1546-1552. <https://doi.org/10.1002/nbm.3609>
20. Manhard MK, Horch RA, Harkins KD, Gochberg DF, Nyman JS, Does MD. Validation of quantitative bound- and pore-water imaging in cortical bone. *Magn Reson Med*. 2014;71(6):2166-2171. <https://doi.org/10.1002/mrm.24870>
21. Zhao X, Song HK, Seifert AC, Li C, Wehrli FW. Feasibility of assessing bone matrix and mineral properties *in vivo* by combined solid-state ^1H and ^{31}P MRI. *PLoS ONE*. 2017;12(3):1-16. <https://doi.org/10.1371/journal.pone.0173995>
22. Nazaran A, Carl M, Ma Y, et al. Three-dimensional adiabatic inversion recovery prepared ultrashort echo time cones (3D IR-UTE-cones) imaging of cortical bone in the hip. *Magn Reson Imaging*. 2017;44:60-64. <https://doi.org/10.1016/j.mri.2017.07.012>
23. Jerban S, Ma Y, Nazaran A, et al. Detecting stress injury (fatigue fracture) in fibular cortical bone using quantitative ultrashort echo time-magnetization transfer (UTE-MT): an *ex vivo* study. *NMR Biomed*. 2018:e3994. <https://doi.org/10.1002/nbm.3994>
24. Diaz E, Chung CB, Bae WC, et al. Ultrashort echo time spectroscopic imaging (UTESI): an efficient method for quantifying bound and free water. *NMR Biomed*. 2012;25(1):161-168. <https://doi.org/10.1002/nbm.1728>
25. Jerban S, Nazaran A, Cheng X, et al. Ultrashort echo time T_2^* values decrease in tendons with application of static tensile loads. *J Biomech*. 2017;61:160-167. <https://doi.org/10.1016/j.jbiomech.2017.07.018>
26. Shao H, Chang EY, Pauli C, et al. UTE bi-component analysis of T_2^* relaxation in articular cartilage. *Osteoarthr Cartil*. 2016;24(2):364-373. <https://doi.org/10.1016/j.joca.2015.08.017>
27. Horch RA, Gochberg DF, Nyman JS, Does MD. Non-invasive predictors of human cortical bone mechanical properties: T_2 -discriminated ^1H NMR compared with high resolution X-ray. *PLoS ONE*. 2011;6(1):1-5. <https://doi.org/10.1371/journal.pone.0016359>
28. Manhard MK, Horch RA, Gochberg DF, Nyman JS, Does MD. *In vivo* quantitative MR imaging of bound and pore water in cortical bone. *Radiology*. 2015;277(1):221-230.
29. Ma YJ, Chang EY, Bydder GM, Du J. Can ultrashort-TE (UTE) MRI sequences on a 3-T clinical scanner detect signal directly from collagen protons: freeze-dry and D_2O exchange studies of cortical bone and Achilles tendon specimens. *NMR Biomed*. 2016;29(7):912-917. <https://doi.org/10.1002/nbm.3547>
30. Chang EY, Bae WC, Shao H, et al. Ultrashort echo time magnetization transfer (UTE-MT) imaging of cortical bone. *NMR Biomed*. 2015;28:873-880. <https://doi.org/10.1002/nbm.3316>
31. Ma Y-J, Chang EY, Carl M, Du J. Quantitative magnetization transfer ultrashort echo time imaging using a time-efficient 3D multispoke cones sequence. *Magn Reson Med*. 2018;79:692-700. <https://doi.org/10.1002/mrm.26716>
32. Springer F, Martirosian P, Machann J, Schwenzer NF, Claussen CD, Schick F. Magnetization transfer contrast imaging in bovine and human cortical bone applying an ultrashort echo time sequence at 3 tesla. *Magn Reson Med*. 2009;61(5):1040-1048. <https://doi.org/10.1002/mrm.21866>
33. Ma Y-J, Tadros A, Du J, Chang EY. Quantitative two-dimensional ultrashort echo time magnetization transfer (2D UTE-MT) imaging of cortical bone. *Magn Reson Med*. 2012;24(3):69-71.
34. Kanberoglu K, Kantarci F, Cebi D, et al. Magnetic resonance imaging in osteomalacic insufficiency fractures of the pelvis. *Clin Radiol*. 2005;60(1):105-111. <https://doi.org/10.1016/j.crad.2004.04.021>
35. Ma Y-J, Lu X, Carl M, et al. Accurate T_1 mapping of short T_2 tissues using a three-dimensional ultrashort echo time cones actual flip angle imaging-variable repetition time (3D UTE-cones AFI-VTR) method. *Magn Reson Med*. 2018;80:598-608. <https://doi.org/10.1002/mrm.27066>
36. Gurney PT, Hargreaves BA, Nishimura DG. Design and analysis of a practical 3D cones trajectory. *Magn Reson Med*. 2006;55(3):575-582. <https://doi.org/10.1002/mrm.20796>
37. Carl M, Bydder GM, Du J. UTE imaging with simultaneous water and fat signal suppression using a time-efficient multispoke inversion recovery pulse sequence. *Magn Reson Med*. 2016;76(2):577-582. <https://doi.org/10.1002/mrm.25823>
38. Ma Y-J, Zhu Y, Lu X, Carl M, Chang EY, Du J. Short T_2 imaging using a 3D double adiabatic inversion recovery prepared ultrashort echo time cones (3D DIR-UTE-cones) sequence. *Magn Reson Med*. 2018;79:2555-2563. <https://doi.org/10.1002/mrm.26908>
39. Mukaka MM. A guide to appropriate use of correlation coefficient in medical research. *Malawi Med J*. 2012;24(3):69-71. <https://doi.org/10.1016/j.cmpb.2016.01.020>
40. Ramani A, Dalton C, Miller DH, Tofts PS, Barker GJ. Precise estimate of fundamental *in-vivo* MT parameters in human brain in clinically feasible times. *Magn Reson Imaging*. 2002;20(10):721-731. [https://doi.org/10.1016/S0730-725X\(02\)00598-2](https://doi.org/10.1016/S0730-725X(02)00598-2)
41. Bae WC, Chen PC, Chung CB, Masuda K, D'Lima D, Du J. Quantitative ultrashort echo time (UTE) MRI of human cortical bone: correlation with porosity and biomechanical properties. *J Bone Miner Res*. 2012;27(4):848-857. <https://doi.org/10.1002/jbmr.1535>
42. Gocha TP, Agnew AM. Spatial variation in osteon population density at the human femoral midshaft: histomorphometric adaptations to habitual load environment. *J Anat*. 2016;228(5):733-745. <https://doi.org/10.1111/joa.12433>

43. Nirody JA, Cheng KP, Parrish RM, et al. Spatial distribution of intracortical porosity varies across age and sex. *Bone*. 2015;75:88-95. <https://doi.org/10.1016/j.bone.2015.02.006>
44. David C, Thomas L, Feik SA, Clement JG. Regional variation of intracortical porosity in the midshaft of the human femur: age and sex differences. *J Anat*. 2005;206:115-125.
45. Hunter RL, Agnew AM. Intraskkeletal variation in human cortical osteocyte lacunar density: implications for bone quality assessment. *Bone Rep*. 2016;5:252-261. <https://doi.org/10.1016/j.bonr.2016.09.002>

How to cite this article: Jerban S, Ma Y, Wan L, et al. Collagen proton fraction from ultrashort echo time magnetization transfer (UTE-MT) MRI modelling correlates significantly with cortical bone porosity measured with micro-computed tomography (μ CT). *NMR in Biomedicine*. 2019;32:e4045. <https://doi.org/10.1002/nbm.4045>